Computers and Geosciences 124 (2019) 93–102

Contents lists available at ScienceDirect

Computers and Geosciences

journal homepage: www.elsevier.com/locate/cageo

Research paper

Downscaling MODIS land surface temperature over a heterogeneous area: An investigation of machine learning techniques, feature selection, and impacts of mixed pixels

Hamid Ebrahimy[1], Mohsen Azadbakht[*,2]

Remote Sensing and GIS Research Centre, Faculty of Earth Sciences, Shahid Beheshti University, Tehran 653641255, Iran

ARTICLE INFO

Keywords:
Downscaling
Land surface temperature
Random forest
Extreme learning machine
MODIS
Feature selection

ABSTRACT

Remotely sensed Land Surface Temperature (LST) is of paramount importance in numerous environmental applications. Although, coarse spatial resolution sensors provide frequent LST measurements, their applicability is rather limited for many applications. Downscaling methods are therefore applied to improve the spatial resolution of LST products. A number of Machine Learning (ML) methods have already been used in the LST downscaling studies. Nevertheless, the literature lacks a suitable inter-comparison of different ML methods, as well as the impact of the feature selection process on downscaling results. This study aims at comparing downscaled LST from 1 km daily MODIS LST product (MOD11A1) to 240 m using Random Forest Regression (RFR), Support Vector Regression (SVR), Extreme Learning Machine (ELM) and Temperature Sharpening (TsHARP) approaches with 11 predictor variables at a heterogeneous area in different seasons. In addition, by implementing a feature selection with the Support Vector Machine-Recursive Feature Elimination (SVM-RFE) method, the most important variables were selected and used as inputs of the models. The results were evaluated against the LST derived from Landsat-8 thermal imageries using a split window method, showing that all the ML methods perform well in LST downscaling (with an average RMSE = 2.5 and MAE = 1.74) with marginal differences, outperforming the TsHARP method (RMSE ~ 3.02, MAE ~ 2.19). Among all the methods, ELM required the least computational effort, and when it was combined with SVM-RFE, general efficiency of the downscaling procedure was increased substantially.

1. Introduction

The retrieved Land Surface Temperature (LST) from satellite imageries has been used in a wide variety of fields, including forest monitoring (Guo and Zhou, 2004; Hansen et al., 2008), burn severity assessment (Quintano et al., 2015; Zheng et al., 2016), land cover change detection (de Beurs et al., 2015; Muster et al., 2015), urban heat island monitoring (Fu and Weng, 2016; Li et al., 2016; Peres et al., 2018), drought assessment and monitoring (Hao et al., 2015; Son et al., 2012), energy balance modeling (Bhattarai et al., 2016; Song et al., 2016) and agricultural studies (de Wit et al., 2004; Marques da Silva et al., 2015). These analyses are often carried out at fine to moderate spatial resolutions, and thus requiring LST measured at relevant spatial scales. However, acquiring LST at high temporal and spatial resolutions from space is challenging and to some extent infeasible, given the orbital configurations and technical considerations of the current satellites. An alternative, and widely adopted in thermal remote sensing studies, is to downscaling LST acquired from coarse spatial resolution imageries through utilizing ancillary data (Atkinson, 2013; Zhan et al., 2013).

Different statistical (Bechtel et al., 2012; Kustas et al., 2003; Zakšek and Oštir, 2012), physical (Liu and Pu, 2008; Liu and Zhu, 2012) and spatio-temporal (Addesso et al., 2015; Moosavi et al., 2015; Weng et al., 2014; Wu et al., 2015) methods have been developed for LST downscaling. Among the various methods, statistical methods have been highly considered due to their simplicity and accuracy (Zhan et al., 2013). Statistical methods generally estimate the relationship between LST and predictor variables at coarse spatial resolution, and this relationship is then applied to high resolution predictor datasets to retrieve LST at fine resolution.

Traditional and well-known statistical methods, such as

* Corresponding author.
E-mail addresses: hamdebrahimy@gmail.com (H. Ebrahimy), m_azadbakht@sbu.ac.ir (M. Azadbakht).
[1] Hamid Ebrahimy designed the research experiments and provided the analyses.
[2] Mohsen Azadbakht supervised the research and contributed to preparation of the manuscript.

https://doi.org/10.1016/j.cageo.2019.01.004
Received 18 August 2018; Received in revised form 5 January 2019; Accepted 8 January 2019
Available online 09 January 2019
0098-3004/

Disaggregation of Radiometric Temperature (DisTrad) (Kustas et al., 2003) and Temperature Sharpening (TsHARP) (Agam et al., 2007) use vegetation indices and linear regression relationships. Nevertheless, despite their simplicity and good results in homogeneous agricultural areas (Agam et al., 2007, 2008) they may not perform well in downscaling LST over heterogeneous and urban areas (Chen et al., 2014; Jeganathan et al., 2011; Mukherjee et al., 2015; Yang et al., 2017b). To address this problem, advanced nonlinear methods and different ancillary datasets such as topographic information, spectral bands, vegetation indices and land cover data have been successfully used in different studies (Bechtel et al., 2012; Bindhu et al., 2013; Ghosh and Joshi, 2014; Liu and Pu, 2008; Liu and Zhu, 2012; Yang et al., 2017b; Zhan et al., 2013). Meanwhile, various Machine Learning (ML) methods such as Regression Trees (RT), Partial Least Square (PLS), Artificial Neural Network (ANN), Support Vector Regression (SVR) and Random Forest Regression (RFR) are also used and they perform well compared to traditional methods such as DisTrad and TsHARP (Gao et al., 2012; Ghosh and Joshi, 2014; Hutengs and Vohland, 2016; Yang et al., 2010, 2011, 2017a). To the best of the author's knowledge, of the ML methods, Extreme Learning Machine (ELM) has not yet been used in LST downscaling, while it has been successfully applied in remote sensing studies (Ding et al., 2015) and analyzing complex spatial problems (Leuenberger and Kanevski, 2015).

In the studies conducted so far, less attention has been paid to the thorough comparison of different ML methods in LST downscaling in order to recommend the most operative method(s). This study evaluates the performance of the selected ML methods (RFR, SVR, and ELM) and TsHARP for downscaling MODIS LST product in a very heterogeneous area and in different seasons, providing a detailed quantitative and visual comparison of the downscaling methods. Furthermore, in order to reduce the computational complexity, a feature selection process based on Support Vector Machine-Recursive Feature Elimination (SVM-RFE) method is applied to select the best predictor variables and use them as model inputs, where finally, an evaluation of downscaling results with and without feature selection is also addressed. In addition, the impact of pixel impurity and heterogeneity on LST downscaling is also investigated.

2. Study area

The study area with an approximate area of 5170 km^2 covers a part of Tehran province in Iran, and it is located between latitudes 35° 37′ N and 35° 59′ N, and longitudes 50° 99′ E and 51° 88′ E (Fig. 1). The altitude of this area decreases significantly from north to south, ranging from 3960 to 867 m above sea level. The study area is covered with five main land covers, where approximately 50% of the area is covered by rangelands, while agricultural areas, residential areas, barelands and water bodies cover 25.5%, 15.5%, 8.5% and 0.5%, respectively. Land cover diversification as well as heterogeneity of the study area in terms of elevation and vegetation status allow comparison of the selected algorithms and may lead to generalize the results to other study areas. In order to analyze the downscaling methods in more details, five spatial subsets are selected in the study area. Subset 1 (S1) includes residential areas with relatively flat topography, subset 2 (S2) is located in agricultural lands with almost similar topographical conditions as in S1. Major part of the subset 3 (S3) is covered by barelands in low altitude areas, subset 4 (S4) contains barelands and water bodies, and subset 5 (S5) is mainly covered by barelands and is located in a mountainous area.

3. Materials and methods

Fig. 2 shows workflow of the present study for downscaling MODIS daily LST product, including initial data collection and preprocessing, Landsat-8 LST retrieval, feature selection, LST downscaling and finally accuracy assessment. Initial data collection and preprocessing consists of acquiring MOD11A1 images and other remotely sensed datasets and performing some pre-processing steps such as resampling and calculation of vegetation indices. Then, Landsat-8 LST is retrieved using a split window method. A feature selection method, SVM-RFE, is then conducted to identify the best predictor variables. The next step involved adopting the ML models (RFR, SVR, and ELM) for downscaling LST at 240 m. Finally, performance evaluation of the methods is carried out using evaluation metrics, visual comparisons and their relationships with the Normalized Difference Vegetation Index (NDVI).

3.1. Data preparation

In order to achieve more reliable results and a more detailed comparison of the selected ML techniques in downscaling LST, three MODIS images of land surface temperature (MOD11A1) from different seasons (Spring, Summer and Autumn) were acquired through the Reverb–Next Generation Earth Science Discovery Tool (http://reverb.echo.nasa.gov/reverb) on June 20 (Spring), on August 7 (Summer), and on November 24 (Autumn) in 2016. Calibrated Landsat-8 Operational Land Imager (OLI) and TIRS images of the same times were also downloaded from the USGS Earth Explorer website (http://earthexplorer.usgs.gov). The MODIS images were then registered to the WGS 84/UTM Zone 39 N coordinate system (same as Landsat-8 images) using the MODIS Reprojection Tool (Dwyer and Schmidt, 2006).

In this study, eleven predictor variables are selected from four main groups including spectral bands, vegetation indices, topographic parameters and land cover for downscaling LST of MOD11A1 from 1 km pixel size to 240 m. These parameters are selected based on the previous studies (Bonafoni, 2016; Gao et al., 2012; Hutengs and Vohland, 2016; Mukherjee et al., 2014; Yang et al., 2017a; Zakšek and Oštir, 2012) and specific conditions of the study area. Selected variables are including the red band, near infrared band, Simple Ratio Index (RVI), Differenced Vegetation Index (DVI), Renormalized Difference Vegetation Index (RDVI), NDVI, Soil Adjusted Vegetation Index (SAVI), Modified Soil Adjusted Vegetation Index (MSAVI), land cover, altitude and Sky view factor (Zakšek et al., 2011). A full description of the selected vegetation indices are available in Bannari et al. (1995). Predictor variables are extracted from the MODIS surface reflectance product (MOD09GQ) (Vermote and Wolfe, 2015), a national land cover data and the ASTER Global Digital Elevation Model2 (GDEM2) (Tachikawa et al., 2011).

In the final step of data preparation, the MOD11A1 LST product is resampled to 960 m cell size using the nearest neighbor method and is used as a dependent variable in fitting the regression models. The predictor variables are also converted to 960 m pixel size serving as inputs to model fitting and to 240 m pixel size for downscaling LST. Some accuracy assessment approaches have already been applied (Rodriguez-Galiano et al., 2012; Zhan et al., 2013), while in this study we use Landsat-8 LST images. The LST of Landsat-8 TIRS images were retrieved using a Split Window method proposed by Jiménez-Muñoz et al. (2014), and they were resampled using the nearest neighbor method to a pixel size of 240 m same as the downscaled LST, for accuracy assessment purposes. Moreover, direct comparison between the downscaled LST and Landsat-8 LST is not possible due to the structural differences between these two types of sensors, thus to convert the Landsat LST to the comparable MODIS LST (Bindhu et al., 2013), inter-sensor conversion coefficients were derived using linear regression from aggregated Landsat LST and MODIS LST at 960 m and were applied on 240 m Landsat LST.

3.2. Feature selection

Support Vector Machine-Recursive Feature Elimination (SVM-RFE) is categorized among the embedded ranking-based methods that selects a fixed number of high-ranking features for subsequent analyzes (Guyon et al., 2002). SVM-RFE has been successfully used in remote sensing studies (Tuia et al., 2009; Zhang et al., 2017). With this method,

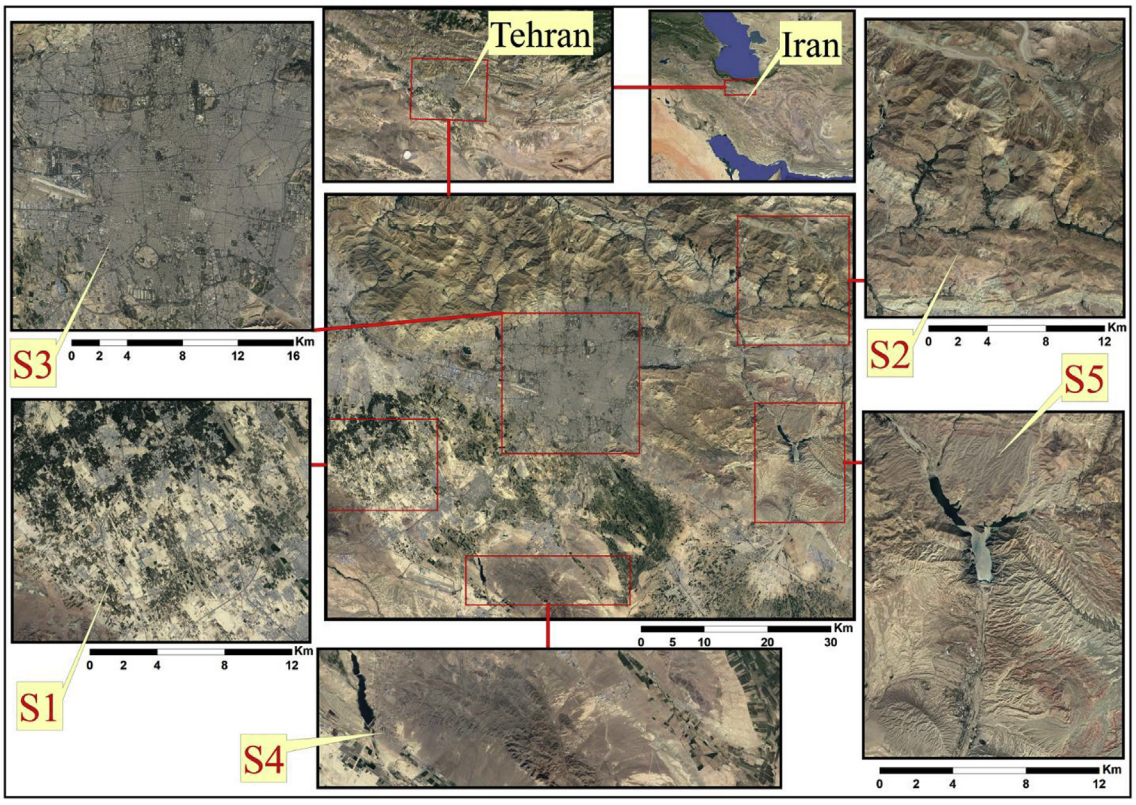

Fig. 1. Study Area with five spatial subsets highlighted.

at first, the current feature subset F contains all the variables. At each iteration, an SVM model is built based on the current feature subset F, the weight ($||w||^2$) of each feature in F is calculated based on analysis of the observed changes in the cost function as a criterion to rank the variables, and then the feature with the smallest ranking score is eliminated (Guyon et al., 2002). This process continues until no further features are remained and a feature ranking list is generated. The full description of this method is available in Guyon et al. (2002). SVM-RFE is implemented within the caret (Kuhn, 2008) and e1071 (Meyer et al., 2017) packages in R environment (R Core Team, 2017). This method is applied for each of the MODIS LST data and predictor variables on different dates. Among the high-ranked features in all different acquisition dates, 3 similar high-ranked variables were chosen as the final variables, namely DEM, NDVI, and the Red band.

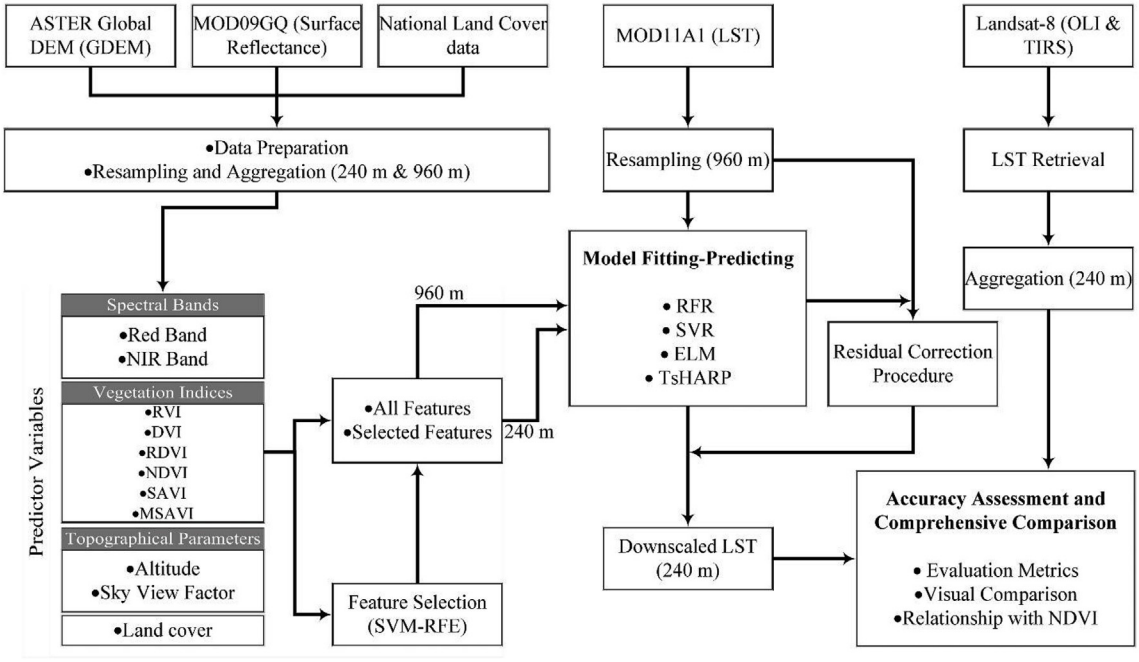

Fig. 2. A schematic workflow of the current study.

3.3. Machine learning methods

3.3.1. Random Forest Regression

Random Forest Regression (RFR) is a powerful ensemble ML method that provides reliable estimates using large number of random and decorrelated decision trees (Belgiu and Drăguţ, 2016; Breiman, 2001) and it has been widely used in regression and classification problems (Aghighi et al., 2018; Azadbakht et al., 2018). Decision trees are growing by generating random subsets with replacement (bootstrap) from training datasets. As an improved form of Classification and Regression Trees (CART) (Liaw and Wiener, 2002), a large collection of decision trees (forest) is used instead of using only one decision tree in order to increase the stability and decrease the sensitivity of the model as well as to avoid over-fitting problems. In RFR, the bootstrap method is used to select a random subset of several variables that describe training samples, and data excluded from this set are called "Out-of-Bag" (OOB) samples, which are usually used in model performance evaluation (Breiman, 2001). In general, to generate an optimal RFR model, it is necessary to tune two parameters, namely ntree (number of decision trees in the forest) and mtry (number of predictor variables on each node of the trees), which lead to achieving the highest possible accuracy of the constructed model. According to the previous studies (Belgiu and Drăguţ, 2016), the numerical ranges of these two parameters were determined and then using a 10-fold cross validation approach, the best values of ntree and mtry were simultaneously identified. The RFR model was built using the randomForest package (Liaw and Wiener, 2002) in R environment.

3.3.2. Support Vector Regression

Support Vector Machine (SVM) is known as a very specific ML algorithm, which has been extensively used in classification and regression problems in various remote sensing studies (Mountrakis et al., 2011). In general, SVM in regression problems called "Support Vector Regression" (SVR) and it uses a kernel function to transfer training data from a lower-dimensional space to a higher-dimensional feature space, where a complex regression problem can be solved linearly (Basak et al., 2007; Mountrakis et al., 2011; Vapnik, 2000). The main purpose of SVR is to fit an optimized function using a subset of training data, called "support vectors", in which all of errors are less than a predefined value () (Smola and Schölkopf, 2004). SVR tries to avoid over-fitting problems and also due to the definition of the algorithm as a convex optimization problem, the convergence occurs at global minima rather than local minima (Schölkopf et al., 2000). So far, various kernel functions, including linear, polynomials, Radial Basis Function (RBF), and Sigmoid have been introduced and developed. In this study, the RBF kernel is selected, in which it is known as the most widely used kernel in remote sensing studies and its performance superiority over other kernels has been reported in previous studies (Mountrakis et al., 2011). In the RBF kernel, selection of high value for the cost parameter (C) leads to an over-fitted model, while gamma values affect the shape of the separator hyper-plane. In this study, the e1071 package (Meyer et al., 2017) in R software was used for SVR implementation with the RBF kernel, and optimal values of the hyper-parameters were determined through adopting 10-fold cross validation.

3.3.3. Extreme Learning Machine

Extreme Learning Machine (ELM) is known as an extended version of the single-hidden layer feed-forward neural networks (SLFNs), which was introduced by Huang et al. (2006). A typical form of ELM consists of a single input layer, a hidden layer, and an output layer. The learning speed of this model is considerably faster than the traditional artificial neural networks, and it also provides much more generalizability and transferability (Ding et al., 2015; Huang et al., 2012). There are also other advantages of ELM, including easy implementation, fast convergence speed and rate, and the ability of modeling highly complex and non-linear processes such as environmental phenomena and modeling of real world issues (Ding et al., 2015; Leuenberger and Kanevski, 2015). In this algorithm, hidden layer weights and biases are randomly generated without an iteratively tuning procedure, while an analytical method determines the weights of the output layer (Huang et al., 2012). A detailed formula and comprehensive description of this method can be found in Huang et al. (2006). In this algorithm, only one meta-parameter (number of hidden neurons) should be tuned by the user to reach the optimum performance of the model, so similar to RFR and SVR, a 10-fold cross validation was used to estimate the optimal meta-parameter. It should be noted that ELM was implemented entirely in R software using the ELMR package (Petrozziello, 2015).

3.4. Downscaling procedure

A ML regression model for downscaling LST is as follows,

$$Y = f(X) \quad (2)$$

where X represents the predictor variables and is the dependent variable (LST), and f symbolizes a non-linear regression function constructed through the training procedure by a ML method. In this study, the relationship between the LST and multiple predictor variables is established on 960 m datasets using the three ML methods. Finally, the developed regression models are applied to 240 m datasets to predict downscaled LST at 240 m cell size. In order to consider the total variation of LST distribution, a residual correction process was adopted to the LST downscaling procedure based on the previous studies (Chen et al., 2014; Jeganathan et al., 2011; Kustas et al., 2003). In this process, a pixel-wise residual value between the predicted model and original MODIS LST in 960 m was calculated, then this 960 m residual was resampled to 240 m, and this residual was finally added to the 240 m downscaled LST from different methods. It should be noted that the TsHARP model was implemented in accordance with the proposed method by Agam et al. (2007), using a moving window of 7 pixels. The quantitative accuracy assessment was performed using two well-known evaluation metrics of regression analysis: Root Mean Square Error (RMSE) and Mean Absolute Error (MAE).

4. Results and discussion

4.1. Downscaling results

The accuracy of the models is presented in Table 1 for the whole study area as well as for the five selected spatial subsets, in terms of the RMSE and MAE. In general, RFR provides better results than ELM, SVR and TsHARP, while the results show that there is a slight difference in the performance of the ML models and there is a remarkable performance superiority of the ML methods over TsHARP. It is interesting to note that, there are slight dissimilarities in the RMSE and MAE values of the ML methods in the downscaled LST of different dates, which in fact represents the high-performance stability of the methods. The overall RMSE values varied from 2.45 to 2.62 °C for RFR, 2.49–2.7 °C for SVR, 2.43–2.64 °C for ELM and 2.94–3.13 °C for TsHARP. The MAE values were around 1.69–1.77 °C for RFR, 1.69–1.82 °C for SVR, 1.67–1.79 °C for ELM and 2.11–2.32 °C for TsHARP.

With regard to the RMSE and MAE values, all the ML methods performed far better than TsHARP. As an example, in the spring image (20/06/2016), for the entire study area, the RMSE and MAE values were decreased by 23%–25% for the ML methods as compared with TsHARP. This improvement is in agreement with other studies, attempted to downscaling LST using regression trees and RFR (Gao et al., 2012; Hutengs and Vohland, 2016).

As shown in Fig. 3, LST in downscaled maps at 240 m share similar patterns and spatial distributions with those of the Landsat-8 LST reference maps and the original MODIS LSTs. More precisely, RFR, SVR and ELM are fairly similar to the reference LSTs, nevertheless all of the methods are in some way incapable of retrieving the full spatial

Table 1
Downscaling accuracy measurement indexes (RMSE and MAE) across all acquisition dates using all features and the selected features over the entire study area and the selected subsets.

Features ↓	Methods	Overall	S1	S2	S3	S4	S5
	↓	RMSE (MAE) °C	RMSE (MAE) °C	RMSE (MAE) °C	RMSE (MAE) °C	RMSE (MAE) °C	RMSE (MAE) °C
20/06/2016							
All features	RFR	2.5 (1.77)	1.23 (0.93)	1.49 (1.21)	1.21 (0.96)	4.97 (3.52)	**2.58 (1.94)**
	SVR	2.55 (1.82)	1.29 (0.99)	1.59 (1.29)	1.48 (1.21)	**4.86 (3.46)**	2.96 (2.17)
	ELM	2.52 (1.79)	1.28 (0.98)	1.53 (1.24)	1.40 (1.15)	4.9 (3.48)	2.91 (2.15)
Selected features	RFR	**2.5 (1.77)**	**1.22 (0.92)**	**1.48 (1.2)**	**1.2 (0.96)**	4.93 (3.48)	2.62 (1.97)
	SVR	2.54 (1.81)	1.28 (0.98)	1.56 (1.27)	1.44 (1.18)	4.89 (3.47)	2.96 (2.17)
	ELM	2.52 (1.78)	1.27 (0.97)	1.53 (1.24)	1.4 (1.15)	4.91 (3.49)	3.01 (2.19)
	TsHARP	3.13 (2.32)	1.75 (1.38)	1.88 (1.49)	1.62 (1.31)	5.24 (3.84)	3.79 (2.95)
07/08/2016							
All features	RFR	**2.61 (1.76)**	**1.06 (0.57)**	2.7 (1.95)	1.42 (1.06)	4.64 (3.54)	2.73 (2.09)
	SVR	2.7 (1.81)	1.23 (0.69)	2.83 (2.06)	1.41 (1.02)	**4.55 (3.5)**	3.06 (2.23)
	ELM	2.64 (1.76)	1.24 (0.72)	**2.69 (1.93)**	1.53 (1.07)	4.64 (3.53)	2.89 (2.18)
Selected features	RFR	2.62 (1.77)	1.13 (0.89)	2.7 (1.93)	1.1 (0.79)	4.57 (3.45)	**2.57 (1.73)**
	SVR	2.64 (1.78)	1.22 (0.95)	2.77 (2.01)	1.2 (0.82)	4.48 (3.37)	2.81 (2.23)
	ELM	2.64 (1.77)	1.3 (1.04)	2.7 (1.95)	**1.09 (0.78)**	4.55 (3.44)	2.76 (1.98)
	TsHARP	3.00 (2.16)	1.33 (0.82)	2.98 (2.24)	2.61 (1.98)	4.76 (3.71)	3.68 (2.94)
24/09/2016							
All features	RFR	2.46 (1.7)	**0.85 (0.59)**	2.13 (1.59)	1.49 (1.19)	4.2 (3.46)	2.84 (2.15)
	SVR	2.49 (1.72)	0.93 (0.65)	2.11 (1.53)	1.55 (1.28)	4.06 (3.31)	2.96 (2.25)
	ELM	**2.43 (1.67)**	0.97 (0.6)	**2.01 (1.45)**	1.63 (1.33)	4.25 (3.47)	2.88 (2.2)
Selected features	RFR	2.45 (1.69)	1.11 (0.81)	2.1 (1.56)	**1.04 (0.69)**	4.07 (3.35)	**2.28 (1.62)**
	SVR	2.46 (1.69)	1.18 (0.86)	2.08 (1.5)	1.14 (0.7)	**3.99 (3.21)**	2.41 (1.72)
	ELM	2.43 (1.67)	1.19 (0.88)	2.01 (1.47)	1.22 (0.73)	4.17 (3.4)	2.33 (1.66)
	TsHARP	2.94 (2.11)	1.08 (0.62)	2.36 (1.78)	2.36 (1.94)	4.33 (3.53)	3.86 (3.12)

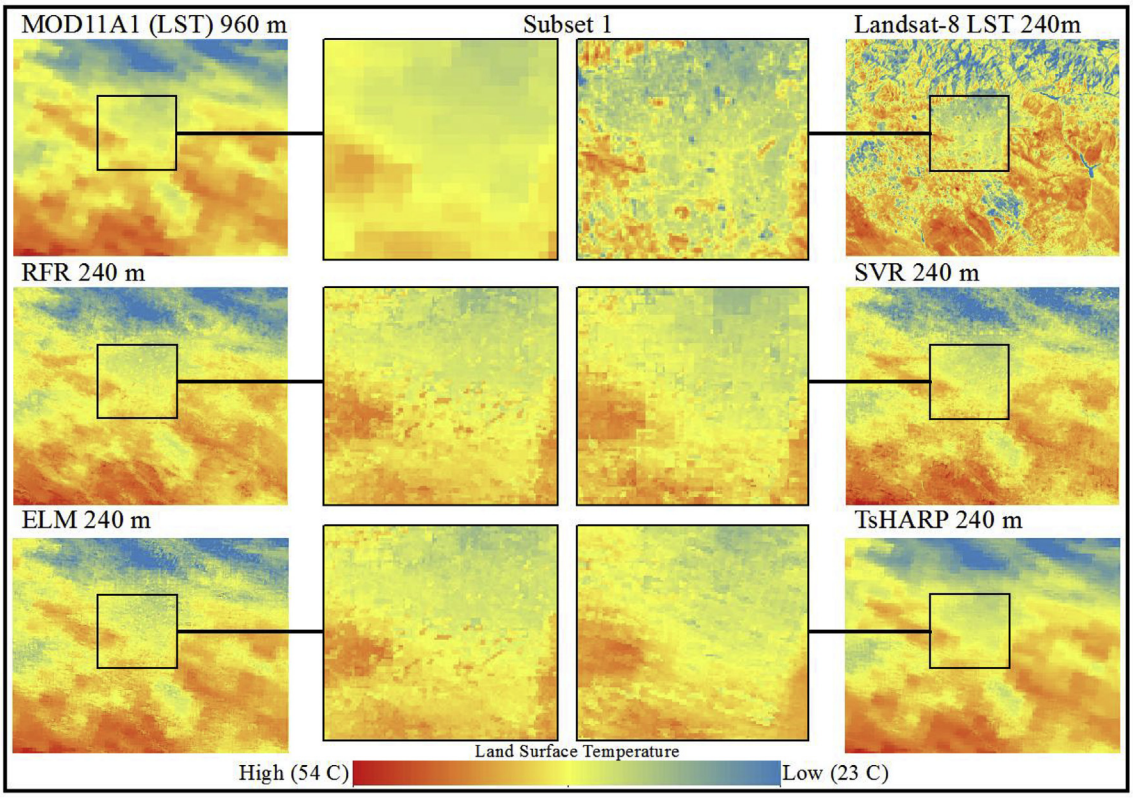

Fig. 3. Comparison of the downscaled LST from different methods (RFR, SVR, ELM, TsHARP) using selected features with the original LST 960 m and Landsat-8 LST 240 m for the acquired image on 07/08/2016.

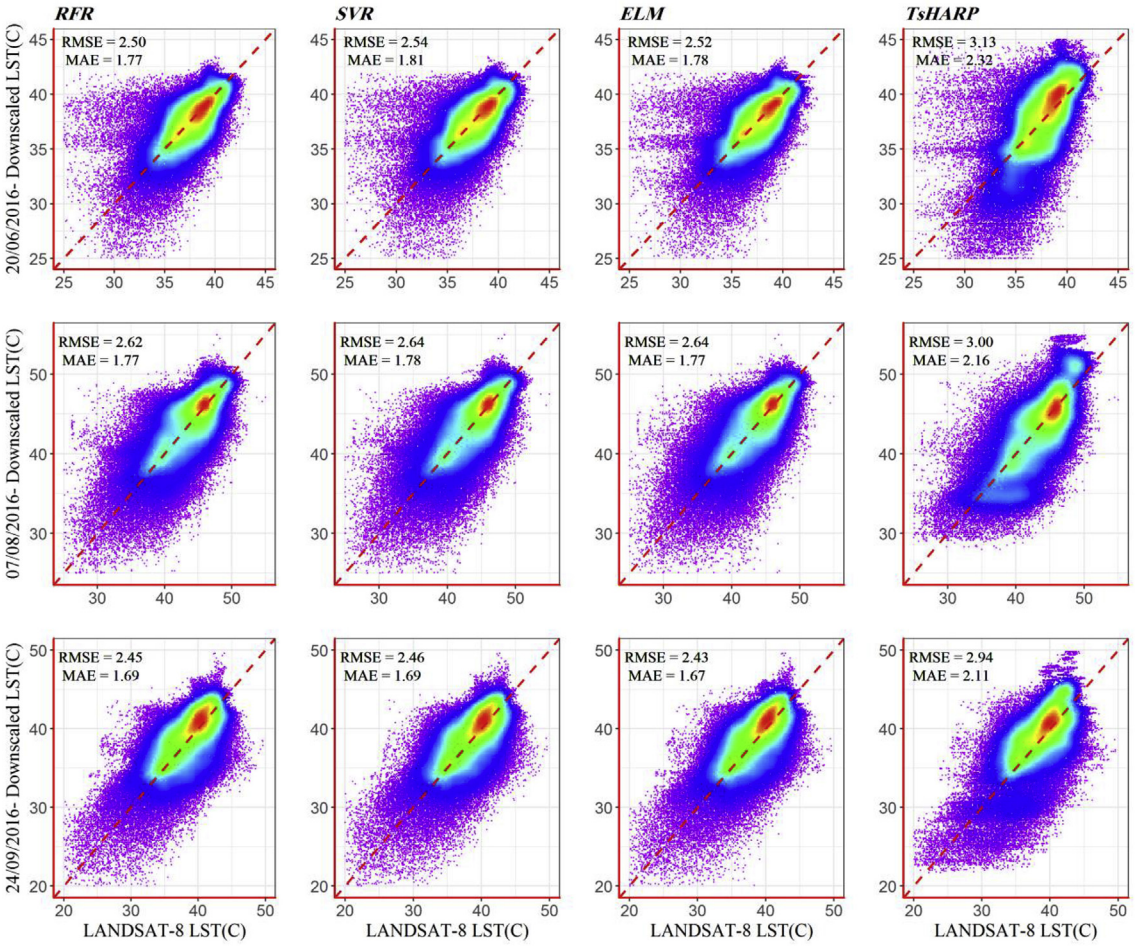

Fig. 4. Scatter plots of per-pixel comparison between Landsat-8 LST 240 m vs. downscaled LST 240 m using the selected features.

variations and distribution of the reference LSTs. RFR, ELM and SVR provided much more detail than TsHARP, as shown in subset 1 (Fig. 3) that could, in turn, provide a great opportunity for investigating temperature conditions in residential areas. Although all the downscaling methods have a relatively large blurring effect compared to the reference LST from Landsat-8, this effect was less evident in the results of the ML techniques as compared to TsHARP. It should also be noted that some of these blurring effects are inevitable and are directly related to the residual correction procedure.

The pixel-based scatter plots of the downscaled LSTs based on the selected features against the reference Landsat LSTs using different methods are presented in Fig. 4. As shown in this Figure, most of the pixels for all the methods follow a 1:1 relationship, while there still exists some pixels with large variations from the 1:1 relationship, either under-predicting or over-predicting the LST values. A detailed investigation of the scatter plots demonstrated that most of the variations from the 1:1 line and outliers were observed in low LST values, occurring in mountainous areas and water bodies. Nevertheless, the point density in the high LST values is much better than the low LST values and there is a good agreement with the 1:1 line. This can demonstrate that the downscaling approaches are more accurate in predicting higher LST values, especially in the range of 35–40 °C as observed in the acquired image in spring season.

According to the results, performance of the ML models on different acquisition dates did not differ substantially after performing feature selection using SVM-RFE, and rather similar results were obtained when using all the predictor variables. Downscaling by all of the selected features as input parameters demands higher computational costs. However, by adopting a feature selection approach and excluding unimportant variables, reduction of the computational time is provided while maintaining similar accuracy levels.

4.2. Comprehensive accuracy assessment

Detailed investigation of the downscaled models with the selected features in the spatial subsets demonstrates that despite the existence of slight differences between the models, it is impossible to introduce a unique model that provides the highest accuracy across all subsets. For more clarification, in subsets 1, 2, and 5 on all dates and in subset 3 from the spring and autumn LST data, the lowest RMSE and MAE were obtained using RFR, while ELM presented the best results for subset 3 in the summer LST data. In subset 4, SVR predicted the downscaled LST at 240 m with the least error rate compared to the other methods on all dates. The possible explanation for these results might be attributed to the characteristics of multiple and complex interactions between the LST and predictive variables, variations in spatial distribution and patterns of LST, and degree of adaptability and flexibility of the selected ML models in different conditions.

Among the subsets, the highest increase in accuracy compared to TsHARP was obtained in subset 5 in autumn using RFR with the selected features. Particularly, the RMSE and MAE values of RFR were boosted about 32% and 34% as compared with TsHARP, respectively. On the other hand, the highest degree of similarity in the accuracy of the ML methods and TsHARP was observed in subset 2. This can be an indication for good performance of TsHARP in fairly homogenous vegetated areas (Agam et al., 2007; Chen et al., 2014; Gao et al., 2012; Jeganathan et al., 2011). Same as the subsets, the evaluation metrics for each of the land cover classes showed that despite very small

Table 2
Per class downscaling accuracy measurement metrics (RMSE and MAE) for all features and the selected features.

Features ↓	Methods ↓	Agricultural area	Bareland	Rangeland	Residential area	Water bodies
		RMSE (MAE) ˚C	RMSE (MAE) ˚C	RMSE (MAE) ˚C	RMSE (MAE) ˚C	RMSE (MAE) ˚C
20/06/2016						
All features	RFR	2.03 (1.44)	1.87 (1.41)	2.94 (2.14)	1.76 (1.23)	5.14 (4.56)
	SVR	2.11 (1.54)	1.86 (1.42)	3.01 (2.2)	1.65 (1.2)	**4.03 (3.61)**
	ELM	2.08 (1.49)	1.82 (1.39)	2.97 (2.17)	1.67 (1.19)	5.37 (4.75)
Selected features	RFR	**2.03 (1.44)**	1.87 (1.41)	**2.93 (2.13)**	1.74 (1.22)	5.21 (4.64)
	SVR	2.09 (1.52)	1.85 (1.41)	3 (2.19)	**1.64 (1.18)**	4.04 (3.64)
	ELM	2.05 (1.47)	**1.82 (1.39)**	2.98 (2.17)	1.66 (1.19)	5.29 (4.79)
	TsHARP	2.42 (1.82)	2.51 (1.88)	3.7 (2.81)	2.14 (1.62)	5.66 (4.99)
07/08/2016						
All features	RFR	2.79 (1.91)	1.89 (1.26)	**2.82 (1.99)**	1.93 (1.12)	5.91 (4.68)
	SVR	2.89 (1.99)	1.82 (1.18)	2.98 (2.07)	1.84 (1.11)	**4.47 (3.36)**
	ELM	2.83 (1.94)	1.81 (1.14)	2.88 (2)	1.85 (1.13)	5.74 (4.42)
Selected features	RFR	**2.79 (1.91)**	1.89 (1.26)	2.84 (2)	1.9 (1.1)	5.84 (4.61)
	SVR	2.87 (1.96)	1.83 (1.18)	2.88 (2.01)	**1.8 (1.07)**	4.95 (3.8)
	ELM	2.85 (1.95)	**1.8 (1.14)**	2.88 (2)	1.82 (1.1)	5.53 (4.32)
	TsHARP	2.79 (1.92)	2.67 (1.84)	3.01 (2.19)	2.06 (1.54)	5.97 (4.81)
24/09/2016						
All features	RFR	**2.06 (1.42)**	2.05 (1.53)	**2.81 (2.01)**	1.78 (1.05)	5.33 (4.2)
	SVR	2.17 (1.49)	1.96 (1.42)	2.9 (2.08)	1.67 (1.01)	**4.28 (3.26)**
	ELM	2.11 (1.45)	1.89 (1.34)	2.84 (2.04)	1.67 (1.02)	5.17 (4.02)
Selected features	RFR	2.06 (1.43)	2.06 (1.53)	2.83 (2.03)	1.75 (1.02)	5.63 (4.69)
	SVR	2.14 (1.47)	1.97 (1.42)	2.86 (2.05)	**1.63 (0.96)**	4.46 (3.65)
	ELM	2.11 (1.45)	**1.89 (1.34)**	2.82 (2.02)	1.64 (0.97)	5.58 (4.66)
	TsHARP	2.26 (1.59)	2.43 (1.83)	3.18 (2.3)	1.81 (1.09)	5.98 (4.92)

differences in error values, some of methods have been more accurate in some land cover classes.

In the LST images of spring and autumn, the highest level of accuracy was recorded for the residential areas, either with all features or the selected ones, where SVR performed better than the rest. However, in the acquired image in summer, the best accuracy was observed in the class barelands by ELM with either all features or the selected ones. More detailed per-class evaluation shows that in all the three acquired images, the highest accuracy in agriculture and rangeland classes is obtained by RFR, while SVR-based downscaled LST with the lowest error rate in residential areas and water bodies. This is justifiable in the case of water bodies due to the ability of this method to achieve maximum accuracy with the limited training data (Mountrakis et al., 2011). The highest accuracy for the bareland areas was achieved by ELM.

As seen in Table 2, the lowest accuracies of the ML methods across different land cover classes were recorded in water bodies, where the RMSE and MAE values were in the range of 5.91 to 4.03 ˚C and 4.81 to 3.61 ˚C, respectively. For the class water bodies, due to the special characteristics of the calculated vegetation index and topographical parameters, it is hardly possible to create an appropriate linear or non-linear regression relationship between the predictor parameters and the LST values. Inappropriate accuracy in such areas has also been reported in other studies (Mukherjee et al., 2014; Yang et al., 2017b). The selected ML methods also had poor accuracy in rangeland areas possibly due to the heterogeneity and complexity of this class which covers a major fraction (50%) of the entire area, and thus having a large variability in terms of the vegetation cover and spatial distribution of LST.

4.3. Comparison of the ML methods

Despite numerous studies on comparing ML methods for classification or regression problems in the remote sensing community, there has not yet been a consensus among various researchers to introduce a specific method that would provide the most appropriate results in all circumstances. In fact, it seems that the general disagreement among the researchers is due to the structural differences between the studies, type of used datasets, heterogeneity levels of the regions, training and testing samples, method of model parameters optimization, accuracy assessment approach and the preprocessing and post-processing steps. On the other hand, in LST downscaling studies it is not sufficient to evaluate the accuracy of the method only, because adoptability of a downscaling procedure depends on the computational complexity in terms of training time and parameter tuning, on the selected features, and on the degree of heterogeneity in the study area.

In terms of overall accuracy, the averaged RMSE and MAE values of the ML methods across all acquisition dates are almost identical, while RFR (RMSE = ~2.52, MAE = ~1.74) provides a marginally higher accuracy than ELM (RMSE = ~2.53, MAE = ~1.74) and SVR (RMSE = ~2.56, MAE = ~1.77). From the standpoint of computational complexity, ELM represents superior performance as compared to RFR and SVR, where high learning speed of this model is due to the random generation of input layer weights and hidden layer biases (Huang et al., 2006, 2012). Moreover, only one meta-parameter should be optimized which in fact leads to the fast adeptness in exploring real world problems with high dimensional datasets, as in downscaling LST. On the other hand, RFR and SVR have more structural complexity than ELM, due to the presence of multiple meta-parameters (e.g. mtry and ntree in RFR; type of kernel, cost function, and gamma in SVR), as well as demanding longer training time (Belgiu and Drăguţ, 2016; Mountrakis et al., 2011; Zhang et al., 2017).

Similarity of the results with all the features and the selected features indicates the ability of the selected ML models in achieving the best possible performance with the most important predictor variables. It seems adopting a feature selection process leads to a significant reduction in primarily preparation steps of the downscaling procedure

and the demanding time for parameter tuning and model training, without imposing a significant influence on the model performance. This will ultimately improve the overall performance of downscaling MODIS LST product at near real-time or automatic applications.

Accuracy of the ML methods using the selected subsets was significantly decreased when heterogeneity or complexity of the topographical conditions and land cover types in the subsets increased. This finding is in agreement with the previous studies (Mukherjee et al., 2015; Yang et al., 2017a). For example, in subset 1 that is located in a fairly homogenous residential area with a flat topography, the highest accuracy of the models was achieved. The lowest accuracies, however, were recorded in subsets 4 and 5 due to the high degrees of heterogeneity in these areas especially in terms of land cover type, topographical conditions as well as the presence of water bodies.

4.4. Relationship of downscaled LST and NDVI

To further evaluate the results, regression analysis was used to determine the best downscaling methods in reconstructing the well-established negative relationship between NDVI and LST. For this purpose, linear regression analysis was conducted to examine the variations of the relationship between LST and NDVI in both the downscaled and reference (Landsat-8) LSTs of 240 m pixel size. Moreover, a chow test was calculated to explore whether the regression coefficients of the downscaled LSTs and those of the reference LSTs were identical (Chow, 1960). The results of this analysis are presented in Table 3. It should be noted that only the results of the downscaled LST using the selected features in subset 3 are presented. The results show that the coefficients of the regression equations extracted from the ML models were comparable to those extracted from the reference LST as compared with the TsHARP method. Closer inspection of the results shows that the regression coefficients and R^2 values were fairly different from those measured using the reference LSTs; however, no significant difference ($p \geq 0.05$) was found between the regression relationships, meaning that the regression models of the downscaled LST and reference LST were equal. In summary, these results confirm the accuracy of these methods, and superiority of the ML models in LST downscaling, which effectively retrieves the existing LST and NDVI relationship at fine spatial resolution.

4.5. Analyzing the heterogeneity effects on LST

To investigate the effects of pixel heterogeneity in terms of land cover composition on the LST values, per pixel fraction of each land cover class in the original MODIS LST (960 m) was calculated and it was used together with the LST values as inputs of a linear regression model. These fraction maps represented land cover types by designating the abundance of each land over in each pixel of the MODIS LST. A detailed land cover map was derived from the Landsat-8 image using Random Forest Classifier, with the overall accuracy being 88% (Kappa = 0.77). The regression coefficients were computed and are presented in Table 4. In total, the results indicate a strong negative correlation between LST and the rangeland and water bodies on one hand, and a strong positive correlation between LST and bareland areas on the other hand, while agricultural and residential areas representing a relatively weak positive correlation with the LST. This form of relationships between LST and land cover fractions could generate a spectrally heterogeneous structure in mixed pixels, with an adverse effect on determining the correct linear or non-linear relationship between LST and predictive parameters. More importantly, this finding leads to the idea that by increasing the pixel impurity, there will be a significant reduction in downscaling capability of different methods, either using linear or non-linear models.

5. Conclusion

In this study, downscaling daily MODIS LST product (MOD11A1) from 1 km to 240 m on three different acquisition dates in a heterogeneous area was investigated through adopting the three selected ML (RFR, SVR, ELM) methods by using 11 predictor variables and 3 selected variables based on a feature selection method (SVM-RFE) in comparison with TsHARP. Moreover, detailed accuracy assessments across different spatial subsets and for land cover classes in the study area were also presented. The ML algorithms outperformed TsHARP in downscaling MOD11A1 LST in terms of quantitative evaluations, visual analyses and retrieval of the existing relationships with NDVI. Evaluation of the methods was carried out using the retrieved LST by a split window method from the Landsat-8 thermal band on the same date. Although the performance measures (RMSE and MAE) indicated that all of the downscaling methods with the exception of TsHARP performed similarly, more detailed analysis revealed that the RFR-based downscaled LST, followed by ELM, yielded the highest prediction accuracy. RFR and ELM were identified as the most accurate methods for downscaling LST on all the acquired dates, where the latter demanded the least model learning, parameter tuning, and computational time as compared to RFR and SVR. Further analysis also showed that the variation of the accuracy metrics (RMSE and MAE) for all of models was consistent with the heterogeneity level presented in the study area. The lowest accuracy was emerged in mountainous areas and water bodies and the highest accuracy was observed in homogeneous residential areas.

Moreover, the accuracy assessment analyses showed slight differences in performance of the ML methods using either all features or the selected features, indicating the good stability of the methods when a feature selection is adopted. Overall, we can conclude that RFR and ELM showed the best overall accuracy and computational efficiency. Moreover, adopting a feature selection method (SVM-RFE) resulted in significant reduction of the required preprocessing steps, increasing the computational simplicity and decreasing training time, which may ultimately increase the overall cost-effectiveness of the LST downscaling procedure. The results of the feature selection procedure also revealed the most informative features including DEM, NDVI, and the Red band, where this finding can offer guidance on the selection of variables for LST downscaling studies.

In the future studies, the suitability of these approaches and extended version of them should be further investigated for low resolution LST images from different sensors in different heterogeneous and homogenous areas. Additional studies with these and other ML methods

Table 3
The regression coefficients of the referenced and downscaled LST with NDVI in subset 3.

Acquired Date →	20/06/2016		07/08/2016		24/09/2016	
Methods ↓	Equation	R^2	Equation	R^2	Equation	R^2
Reference LST	−12.3 × NDVI + 41.8	0.29	−24.5 × NDVI + 50.7	0.33	−17.4 × NDVI + 44.1	0.34
RFR LST	−9.5 × NDVI + 41.4	0.19	−8.1 × NDVI + 49.3	0.19	−7.5 × NDVI + 44.2	0.26
SVR LST	−7.1 × NDVI + 40.8	0.17	−6.5 × NDVI + 49.2	0.15	−8.2 × NDVI + 44.3	0.25
ELM LST	−8.6 × NDVI + 40.6	0.17	−7.8 × NDVI + 49.1	0.14	−5.7 × NDVI + 44.2	0.21
TsHARP LST	−16.3 × NDVI + 40.9	0.14	−4.3 × NDVI + 49.1	0.11	−4.5 × NDVI + 44.1	0.16

Table 4
Linear regression coefficients for MODIS LST 960 m (°C) and land cover fractions.

Date	intercept	Coefficient				
		Agricultural area	Bareland	Rangeland	Residential area	Water body
06/20/2016	36.837	1.43	3.84	−1.17	0.77	−5.15
07/08/2016	43.37	1.08	6.75	−3.29	1.9	−9.57
24/09/2016	36.26	0.4	5.03	−3	0.94	−7.65

with sensitivity and uncertainty analysis of results are also expected to investigate model performances and accuracy improvement. Further research could also be conducted to investigate possible methods for mitigating the blurring effect on the downscaled LST.

Acknowledgement

This research was funded by grants of Shahid Beheshti University (Research contract number 600/1082).

Appendix A. Supplementary data

Supplementary data to this article can be found online at https://doi.org/10.1016/j.cageo.2019.01.004.

References

Addesso, P., Longo, M., Maltese, A., Restaino, R., Vivone, G., 2015. Batch Methods for Resolution Enhancement of TIR Image Sequences. IEEE J. Sel. Top. Appl. Earth Obs. Remote Sens. 8, 3372–3385. https://doi.org/10.1109/JSTARS.2015.2440333.

Agam, N., Kustas, W.P., Anderson, M.C., Li, F., Colaizzi, P.D., 2008. Utility of thermal image sharpening for monitoring field-scale evapotranspiration over rainfed and irrigated agricultural regions. J. Geophys. Res. 35. https://doi.org/10.1029/2007GL032195.

Agam, N., Kustas, W.P., Anderson, M.C., Li, F., Neale, C.M.U., 2007. A vegetation index based technique for spatial sharpening of thermal imagery. Remote Sens. Environ. 107, 545–558. https://doi.org/10.1016/j.rse.2006.10.006.

Aghighi, H., Azadbakht, M., Ashourloo, D., Shahrabi, H.S., Radiom, S., 2018. Machine Learning Regression Techniques for the Silage Maize Yield Prediction Using Time-Series Images of Landsat 8 OLI. IEEE J. Sel. Top. Appl. Earth Obs. Remote Sens. 1–15. https://doi.org/10.1109/JSTARS.2018.2823361.

Atkinson, P.M., 2013. Downscaling in remote sensing. Int. J. Appl. Earth Obs. Geoinf. 22, 106–114. https://doi.org/10.1016/j.jag.2012.04.012.

Azadbakht, M., Fraser, C.S., Khoshelham, K., 2018. Synergy of sampling techniques and ensemble classifiers for classification of urban environments using full-waveform LiDAR data. Int. J. Appl. Earth Obs. Geoinf. 73, 277–291. https://doi.org/10.1016/j.jag.2018.06.009.

Bannari, A., Morin, D., Bonn, F., Huete, A.R., 1995. A review of vegetation indices. Rem. Sens. Rev. 13, 95–120. https://doi.org/10.1080/02757259509532298.

Basak, D., Pal, S., Patranabis, D.C., 2007. Support vector regression. Neural Inf. Process. Lett. Rev. 11, 203–224.

Bechtel, B., Zakšek, K., Hoshyaripour, G., 2012. Downscaling Land Surface Temperature in an Urban Area: A Case Study for Hamburg, Germany. Rem. Sens. 4, 3184. https://doi.org/10.3390/rs4103184.

Belgiu, M., Drăguţ, L., 2016. Random forest in remote sensing: A review of applications and future directions. ISPRS J. Photogrammetry Remote Sens. 114, 24–31. https://doi.org/10.1016/j.isprsjprs.2016.01.011.

Bhattarai, N., Shaw, S.B., Quackenbush, L.J., Im, J., Niraula, R., 2016. Evaluating five remote sensing based single-source surface energy balance models for estimating daily evapotranspiration in a humid subtropical climate. Int. J. Appl. Earth Obs. Geoinf. 49, 75–86. https://doi.org/10.1016/j.jag.2016.01.010.

Bindhu, V.M., Narasimhan, B., Sudheer, K.P., 2013. Development and verification of a non-linear disaggregation method (NL-DisTrad) to downscale MODIS land surface temperature to the spatial scale of Landsat thermal data to estimate evapotranspiration. Remote Sens. Environ. 135, 118–129. https://doi.org/10.1016/j.rse.2013.03.023.

Bonafoni, S., 2016. Downscaling of Landsat and MODIS Land Surface Temperature Over the Heterogeneous Urban Area of Milan. IEEE J. Sel. Top. Appl. Earth Obs. Remote Sens. 9, 2019–2027. https://doi.org/10.1109/JSTARS.2016.2514367.

Breiman, L., 2001. Random Forests. Mach. Learn. 45, 5–32. https://doi.org/10.1023/a:1010933404324.

Chen, X., Li, W., Chen, J., Rao, Y., Yamaguchi, Y., 2014. A Combination of TsHARP and Thin Plate Spline Interpolation for Spatial Sharpening of Thermal Imagery. Rem. Sens. 6, 2845–2863. https://doi.org/10.3390/rs6042845.

Chow, G.C., 1960. Tests of Equality Between Sets of Coefficients in Two Linear Regressions. Econometrica 28, 591–605. https://doi.org/0.2307/1910133.

de Beurs, K.M., Henebry, G.M., Owsley, B.C., Sokolik, I., 2015. Using multiple remote sensing perspectives to identify and attribute land surface dynamics in Central Asia 2001–2013. Remote Sens. Environ. 170, 48–61. https://doi.org/10.1016/j.rse.2015.08.018.

de Wit, A.J.W., Boogaard, H.L., van Diepen, C.A., 2004. Using NOAA–AVHRR estimates of land surface temperature for regional agrometeorogical modelling. Int. J. Appl. Earth Obs. Geoinf. 5, 187–204. https://doi.org/10.1016/j.jag.2004.03.003.

Ding, S., Zhao, H., Zhang, Y., Xu, X., Nie, R., 2015. Extreme learning machine: algorithm, theory and applications. Artif. Intell. Rev. 44, 103–115. https://doi.org/10.1007/s10462-013-9405-z.

Dwyer, J., Schmidt, G., 2006. The MODIS Reprojection Tool. In: In: Qu, J.J., Gao, W., Kafatos, M., Murphy, R.E., Salomonson, V.V. (Eds.), Earth Science Satellite Remote Sensing, vol. 2. Data, Computational Processing, and Tools. Springer Berlin Heidelberg, Berlin, Heidelberg, pp. 162–177.

Fu, P., Weng, Q., 2016. A time series analysis of urbanization induced land use and land cover change and its impact on land surface temperature with Landsat imagery. Remote Sens. Environ. 175, 205–214. https://doi.org/10.1016/j.rse.2015.12.040.

Gao, F., Kustas, W., Anderson, M., 2012. A Data Mining Approach for Sharpening Thermal Satellite Imagery over Land. Rem. Sens. 4, 3287–3319. https://doi.org/10.3390/rs4113287.

Ghosh, A., Joshi, P.K., 2014. Hyperspectral imagery for disaggregation of land surface temperature with selected regression algorithms over different land use land cover scenes. ISPRS J. Photogrammetry Remote Sens. 96, 76–93. https://doi.org/10.1016/j.isprsjprs.2014.07.003.

Guo, G., Zhou, M., 2004. Using MODIS land surface temperature to evaluate forest fire risk of northeast China. IEEE Geosci. Remote Sens. Lett. 1, 98–100. https://doi.org/10.1109/LGRS.2004.826550.

Guyon, I., Weston, J., Barnhill, S., Vapnik, V., 2002. Gene Selection for Cancer Classification using Support Vector Machines. Mach. Learn. 46, 389–422. https://doi.org/10.1023/A:1012487302797.

Hansen, M.C., Roy, D.P., Lindquist, E., Adusei, B., Justice, C.O., Altstatt, A., 2008. A method for integrating MODIS and Landsat data for systematic monitoring of forest cover and change in the Congo Basin. Remote Sens. Environ. 112, 2495–2513. https://doi.org/10.1016/j.rse.2007.11.012.

Hao, C., Zhang, J., Yao, F., 2015. Combination of multi-sensor remote sensing data for drought monitoring over Southwest China. Int. J. Appl. Earth Obs. Geoinf. 35, 270–283. https://doi.org/10.1016/j.jag.2014.09.011.

Huang, G.B., Zhou, H., Ding, X., Zhang, R., 2012. Extreme Learning Machine for Regression and Multiclass Classification. IEEE Trans. Syst. Man Cybernetic B. 42, 513–529. https://doi.org/10.1109/TSMCB.2011.2168604.

Huang, G.B., Zhu, Q.Y., Siew, C.K., 2006. Extreme learning machine: Theory and applications. Neurocomputing 70, 489–501. https://doi.org/10.1016/j.neucom.2005.12.126.

Hutengs, C., Vohland, M., 2016. Downscaling land surface temperatures at regional scales with random forest regression. Remote Sens. Environ. 178, 127–141. https://doi.org/10.1016/j.rse.2016.03.006.

Jeganathan, C., Hamm, N.A.S., Mukherjee, S., Atkinson, P.M., Raju, P.L.N., Dadhwal, V.K., 2011. Evaluating a thermal image sharpening model over a mixed agricultural landscape in India. Int. J. Appl. Earth Obs. Geoinf. 13, 178–191. https://doi.org/10.1016/j.jag.2010.11.001.

Jiménez-Muñoz, J.C., Sobrino, J.A., Skoković, D., Mattar, C., Cristóbal, J., 2014. Land Surface Temperature Retrieval Methods From Landsat-8 Thermal Infrared Sensor Data. IEEE Geosci. Remote Sens. Lett. 11, 1840–1843. https://doi.org/10.1109/LGRS.2014.2312032.

Kuhn, M., 2008. Building Predictive Models in R Using the caret Package. 28. pp. 1–26. 2008. https://doi.org/10.18637/jss.v028.i05.

Kustas, W.P., Norman, J.M., Anderson, M.C., French, A.N., 2003. Estimating subpixel surface temperatures and energy fluxes from the vegetation index–radiometric temperature relationship. Remote Sens. Environ. 85, 429–440. https://doi.org/10.1016/S0034-4257(03)00036-1.

Leuenberger, M., Kanevski, M., 2015. Extreme Learning Machines for spatial environmental data. Comput. Geosci. 85, 64–73. https://doi.org/10.1016/j.cageo.2015.06.020.

Li, X., Li, W., Middel, A., Harlan, S.L., Brazel, A.J., Turner, B.L., 2016. Remote sensing of the surface urban heat island and land architecture in Phoenix, Arizona: Combined effects of land composition and configuration and cadastral–demographic–economic factors. Remote Sens. Environ. 174, 233–243. https://doi.org/10.1016/j.rse.2015.12.022.

Liaw, A., Wiener, M., 2002. Classification and regression by randomForest. R. News 2, 18–22.

Liu, D., Pu, R., 2008. Downscaling Thermal Infrared Radiance for Subpixel Land Surface Temperature Retrieval. Sensors 8, 2695.

Liu, D., Zhu, X., 2012. An Enhanced Physical Method for Downscaling Thermal Infrared Radiance. IEEE Geosci. Remote Sens. Lett. 9, 690–694. https://doi.org/10.1109/LGRS.2011.2178814.

Marques da Silva, J.R., Damásio, C.V., Sousa, A.M.O., Bugalho, L., Pessanha, L., Quaresma, P., 2015. Agriculture pest and disease risk maps considering MSG satellite data and land surface temperature. Int. J. Appl. Earth Obs. Geoinf. 38, 40–50. https://doi.org/10.1016/j.jag.2014.12.016.

Meyer, D., Dimitriadou, E., Hornik, K., Weingessel, A., Leisch, F., 2017. The e1071 package. Misc Functions of Department of Statistics, Probability Theory Group (Formerly: E1071). TU Wien. https://CRAN.R-project.org/package=e1071.

Moosavi, V., Talebi, A., Mokhtari, M.H., Shamsi, S.R.F., Niazi, Y., 2015. A wavelet-artificial intelligence fusion approach (WAIFA) for blending Landsat and MODIS surface temperature. Remote Sens. Environ. 169, 243–254. https://doi.org/10.1016/j.rse.2015.08.015.

Mountrakis, G., Im, J., Ogole, C., 2011. Support vector machines in remote sensing: A review. ISPRS J. Photogrammetry Remote Sens. 66, 247–259. https://doi.org/10.1016/j.isprsjprs.2010.11.001.

Mukherjee, S., Joshi, P.K., Garg, R.D., 2014. A comparison of different regression models for downscaling Landsat and MODIS land surface temperature images over heterogeneous landscape. Adv. Space Res. 54, 655–669. https://doi.org/10.1016/j.asr.2014.04.013.

Mukherjee, S., Joshi, P.K., Garg, R.D., 2015. Regression-Kriging Technique to Downscale Satellite-Derived Land Surface Temperature in Heterogeneous Agricultural Landscape. IEEE J. Sel. Top. Appl. Earth Obs. Remote Sens. 8, 1245–1250. https://doi.org/10.1109/JSTARS.2015.2396032.

Muster, S., Langer, M., Abnizova, A., Young, K.L., Boike, J., 2015. Spatio-temporal sensitivity of MODIS land surface temperature anomalies indicates high potential for large-scale land cover change detection in Arctic permafrost landscapes. Remote Sens. Environ. 168, 1–12. https://doi.org/10.1016/j.rse.2015.06.017.

Peres, L.d.F., Lucena, A.J.d., Rotunno Filho, O.C., França, J.R.d.A., 2018. The urban heat island in Rio de Janeiro, Brazil, in the last 30 years using remote sensing data. Int. J. Appl. Earth Obs. Geoinf. 64, 104–116. https://doi.org/10.1016/j.jag.2017.08.012.

Petrozziello, A., 2015. ELMR: Extreme Machine Learning (ELM). R package version 1.0. https://CRAN.R-project.org/package=ELMR.

Quintano, C., Fernández-Manso, A., Calvo, L., Marcos, E., Valbuena, L., 2015. Land surface temperature as potential indicator of burn severity in forest Mediterranean ecosystems. Int. J. Appl. Earth Obs. Geoinf. 36, 1–12. https://doi.org/10.1016/j.jag.2014.10.015.

R Core Team, 2017. R: A language and Environment for Statistical Computing. R Foundation for Statistical Computing, Austria, Vienna.

Rodriguez-Galiano, V., Pardo-Iguzquiza, E., Sanchez-Castillo, M., Chica-Olmo, M., Chica-Rivas, M., 2012. Downscaling Landsat 7 ETM+ thermal imagery using land surface temperature and NDVI images. Int. J. Appl. Earth Obs. Geoinf. 18, 515–527. https://doi.org/10.1016/j.jag.2011.10.002.

Schölkopf, B., Smola, A.J., Williamson, R.C., Bartlett, P.L., 2000. New Support Vector Algorithms. Neural Comput. 12, 1207–1245. https://doi.org/10.1162/089976600300015565.

Smola, A.J., Schölkopf, B., 2004. A tutorial on support vector regression. Stat. Comput. 14, 199–222. https://doi.org/10.1023/b:stco.0000035301.49549.88.

Son, N.T., Chen, C.F., Chen, C.R., Chang, L.Y., Minh, V.Q., 2012. Monitoring agricultural drought in the Lower Mekong Basin using MODIS NDVI and land surface temperature data. Int. J. Appl. Earth Obs. Geoinf. 18, 417–427. https://doi.org/10.1016/j.jag.2012.03.014.

Song, L., Liu, S., Kustas, W.P., Zhou, J., Xu, Z., Xia, T., Li, M., 2016. Application of remote sensing-based two-source energy balance model for mapping field surface fluxes with composite and component surface temperatures. Agric. For. Meteorol. 230–231, 8–19. https://doi.org/10.1016/j.agrformet.2016.01.005.

Tachikawa, T., Kaku, M., Iwasaki, A., Gesch, D.B., Oimoen, M.J., Zhang, Z., Danielson, J.J., Krieger, T., Curtis, B., Haase, J., Abrams, M., Carabajal, C., 2011. ASTER Global Digital Elevation Model Version 2 - summary of validation results, second ed. pp. 27. http://pubs.er.usgs.gov/publication/70005960.

Tuia, D., Pacifici, F., Kanevski, M., Emery, W.J., 2009. Classification of Very High Spatial Resolution Imagery Using Mathematical Morphology and Support Vector Machines. IEEE Trans. Geosci. Rem. Sens. 47, 3866–3879. https://doi.org/10.1109/TGRS.2009.2027895.

Vapnik, V., 2000. The Nature of Statistical Learning Theory. Springer-Verlag, New York.

Vermote, E., Wolfe, R., 2015. MOD09GQ: MODIS/Terra Surface Reflectance Daily L2G Global 250 m SIN Grid V006. Available online: https://lpdaac.usgs.gov/dataset_discovery/modis/modis_products_table/mod09gq_v006, Accessed date: 25 January 2018. https://doi.org/10.5067/MODIS/MOD09GQ.006.

Weng, Q., Fu, P., Gao, F., 2014. Generating daily land surface temperature at Landsat resolution by fusing Landsat and MODIS data. Remote Sens. Environ. 145, 55–67. https://doi.org/10.1016/j.rse.2014.02.003.

Wu, P., Shen, H., Zhang, L., Göttsche, F.-M., 2015. Integrated fusion of multi-scale polar-orbiting and geostationary satellite observations for the mapping of high spatial and temporal resolution land surface temperature. Remote Sens. Environ. 156, 169–181. https://doi.org/10.1016/j.rse.2014.09.013.

Yang, G., Pu, R., Huang, W., Wang, J., Zhao, C., 2010. A Novel Method to Estimate Subpixel Temperature by Fusing Solar-Reflective and Thermal-Infrared Remote-Sensing Data With an Artificial Neural Network. IEEE Trans. Geosci. Rem. Sens. 48, 2170–2178. https://doi.org/10.1109/TGRS.2009.2033180.

Yang, G., Pu, R., Zhao, C., Huang, W., Wang, J., 2011. Estimation of subpixel land surface temperature using an endmember index based technique: A case examination on ASTER and MODIS temperature products over a heterogeneous area. Remote Sens. Environ. 115, 1202–1219. https://doi.org/10.1016/j.rse.2011.01.004.

Yang, Y., Cao, C., Pan, X., Li, X., Zhu, X., 2017a. Downscaling Land Surface Temperature in an Arid Area by Using Multiple Remote Sensing Indices with Random Forest Regression. Rem. Sens. 9. https://doi.org/10.3390/rs9080789.

Yang, Y., Li, X., Pan, X., Zhang, Y., Cao, C., 2017b. Downscaling Land Surface Temperature in Complex Regions by Using Multiple Scale Factors with Adaptive Thresholds. Sensors 17. https://doi.org/10.3390/s17040744.

Zakšek, K., Oštir, K., 2012. Downscaling land surface temperature for urban heat island diurnal cycle analysis. Remote Sens. Environ. 117, 114–124. https://doi.org/10.1016/j.rse.2011.05.027.

Zakšek, K., Oštir, K., Kokalj, Ž., 2011. Sky-View Factor as a Relief Visualization Technique. Rem. Sens. 3, 398–415. https://doi.org/10.3390/rs3020398.

Zhan, W., Chen, Y., Zhou, J., Wang, J., Liu, W., Voogt, J., Zhu, X., Quan, J., Li, J., 2013. Disaggregation of remotely sensed land surface temperature: Literature survey, taxonomy, issues, and caveats. Remote Sens. Environ. 131, 119–139. https://doi.org/10.1016/j.rse.2012.12.014.

Zhang, T., Huang, X., Wen, D., Li, J., 2017. Urban Building Density Estimation From High-Resolution Imagery Using Multiple Features and Support Vector Regression. IEEE J. Sel. Top. Appl. Earth Obs. Remote Sens. 10, 3265–3280. https://doi.org/10.1109/JSTARS.2017.2669217.

Zheng, Z., Zeng, Y., Li, S., Huang, W., 2016. A new burn severity index based on land surface temperature and enhanced vegetation index. Int. J. Appl. Earth Obs. Geoinf. 45, 84–94. https://doi.org/10.1016/j.jag.2015.11.002.